SMR.703 - 28

WORKING PARTY ON
MECHANICAL PROPERTIES OF INTERFACES

23 AUGUST - 3 SEPTEMBER 1993

"Mechanical Properties of Metal-Ceramic Interfaces"
Part IV

J. DE HOSSON
University of Groningen
Department of Applied Physics
Nijenborgh 18
Groningen AG 9747
NETHERLANDS

These are preliminary lecture notes, intended only for distribution to participants.

MARTENSITIC TRANSFORMATIONS IN LASER PROCESSED COATINGS

M. van den BURG and J. Th. M. De HOSSON

Department of Applied Physics, Materials Science Centre, University of Groningen, Nijenborgh 4, 9749 AG Groningen, The Netherlands

MARTENSITIC TRANSFORMATIONS IN LASER PROCESSED COATINGS

M. van den BURG and J. Th. M. De HOSSON

Department of Applied Physics, Materials Science Centre, University of Groningen, Nijenborgh 4,
9747 AG Groningen, The Netherlands

Abstract—This paper concentrates on laser coating of Fe–22 wt% Cr and a duplex steel SAF2205 by injecting Cr_2O_3 powder into the melt pool. In particular the work focuses on the stabilization of high temperature distorted spinel phases due to the high quench rates involved as well as on the a quantitative crystallographic analysis of the resulting morphologies. The microstructure observed in TEM indicates that the material does not solidify in the distorted spinel structure. The presence of a small amount of cubic (Fe, Cr)-spinel suggests that the distorted spinel in fact might be nucleated from the cubic spinel phase. The plate like morphology of the distorted spinel phase in combination with the twinned internal structure of the plates put forward the idea that the transformation might be martensitic. Martensitic calculations executed with the lattice parameters of the cubic and distorted (Fe, Cr)-spinel phases are in excellent agreement with the experimental data confirming that the transformation might be martensitic indeed.

1. INTRODUCTION

Many successful wear resisting materials consist of particles of a hard phase dispersed in a more ductile matrix. Such dispersions can be prepared by powder metallurgy techniques or by solidification of an eutectic structure from a melt. Coatings of the former type can only be applied by spray processes because it is necessary to avoid commingling of the components in the molten state. However, the coatings remain separated from the substrate by a sharp interface which is always a potential source of weakness. In the latter type of materials prepared from a melt, the proportion of hard phase is controlled by thermodynamics. The corrosion protection of materials used in industrial environments usually relies on the formation of Cr_2O_3, SiO_2 or Al_2O_3 surface layers. The protection can be hampered by the diffusion of constituents (the alloy or the environment) along grain boundaries. Possible ways to circumvent these problems are to make poreless ceramic coatings or amorphous coatings.

A different approach, followed in this paper, is to modify the surface layer by using a laser beam. Because of its high energy density, the laser beam is able to melt the metallic substrate and may even partly melt the ceramic powder. As a result, a solid bonding can be formed between the ceramic and the metal. However, as the physical properties between ceramic and metallic materials are much different, e.g. the thermal expansion coefficients and the crystallographic structures, cracks usually develop at the interface as well as inside the clad layer during the rapid solidification and cooling processes. Obviously, a good adhesion may prevent the formation of cracks. In addition chemical reactions between ceramics and metals may lead to a good wetting.

In previous publications [1, 2] we reported about the characteristic features of coating a duplex steel SAF 2205 and stainless steel 304 by bringing a mixture of Cr_2O_3 and Fe powder into a laser beam. A powder mixture of Cr_2O_3 and pure iron was brought into the laser beam in order to form a spinel structure inside the coating. Further, it turned out that it is possible to form a thick and homogeneous ceramic coating of Cr_2O_3 on steel by a proper selection of coating parameters such as scanning velocity, overlap and number of layers. A higher laser scan velocity may decrease the convection speed and prevents cracks in the coating induced by the convection. More than 50% overlap is needed in order to compensate for the lack of coating material in the centre of the track being swept away by convection.

In contrast this paper deals with a different substrate and a different coating i.e. Fe–22 wt% Cr and a duplex steel SAF2205 are coated only with Cr_2O_3 by laser injecting the powder into the melt pool. The work concentrates on the stabilization of high temperature distorted spinel phases due to the high quench rates involved as well as on the a quantitative crystallographic analysis of the resulting morphologies.

2. EXPERIMENT

Fe–22 wt% Cr and a duplex steel SAF2205 (see Table 1) were coated with Cr_2O_3 by laser injecting Cr_2O_3 powder into the melt pool of these substrate materials. The size distribution of the Cr_2O_3 particles peaked around 10 μm. For the laser treatment a

Table 1. Chemical composition (nominal) of duplex SAF2205 (wt%)[15]

C	Si	Mn	Cr	Ni	Mo
0.03	1.0	2.0	22	5.5	3.0

CW–CO₂ laser (Spectra Physics 820) was used. The operating conditions were: 1.0 kW laser power, a spot size of 0.75 mm and a laser scan velocity of 20 mm/s. The overlap between the successive laser tracks was 75%. It turned out that the resulting phases and the composition of these phases was not very sensitive to these operating conditions.

X-ray diffraction technique was applied to identify the phases in the laser processed material. The peak intensity positions of the cubic (Fe, Cr)-spinel and the tetragonally distorted (Fe, Cr)-spinel were taken to refine the lattice parameters of these phase. The data for the cubic spinel FeCr₂O₄ and for the distorted spinel Cr₃O₄ were employed as starting values in the calculation of the lattice parameters. The Cr₂O₃ peaks that were always present, were used as an internal calibration of the X-ray diffractometer.

In addition, cross sectional SEM and light microscopy techniques were applied to study the microstructure of the coating. The microstructure could be revealed by etching in modified Groesbeck's reagent. EDS (energy dispersive X-ray spectrometry) was

applied to determine the chemical composition of the (Fe, Cr)-spinel phases.

Transmission electron microscopy was employed to measure the lattice parameters of the spinel phases on a microscopic scale and to reveal microstructural features. Specimens were observed in a JEM200CX transmission electron microscope operating at 200 kV. TEM specimens were made by ultra sonic disc cutting of 3 mm samples followed by dimpling to a final thickness of about 40 μm and thinned by ion milling afterwards. Cross sectional specimens were also made but the observed microstructure turned out to be relatively insensitive to the position in the coating.

3. RESULTS

3.1. X-ray diffraction

X-ray diffraction showed that the predominant phase in the ceramic coating is the tetragonally distorted (Fe, Cr)-spinel phase (Fig. 1). Only small amounts of Cr₂O₃ were found to be present which were due to the Cr₂O₃ particles entering the melt pool too late to become completely melted. Beside the Cr₂O₃ small amounts of cubic (Fe, Cr)-spinel were found as well. These phases are in agreement with predictions from the Fe–Cr–O ternary phase diagram.
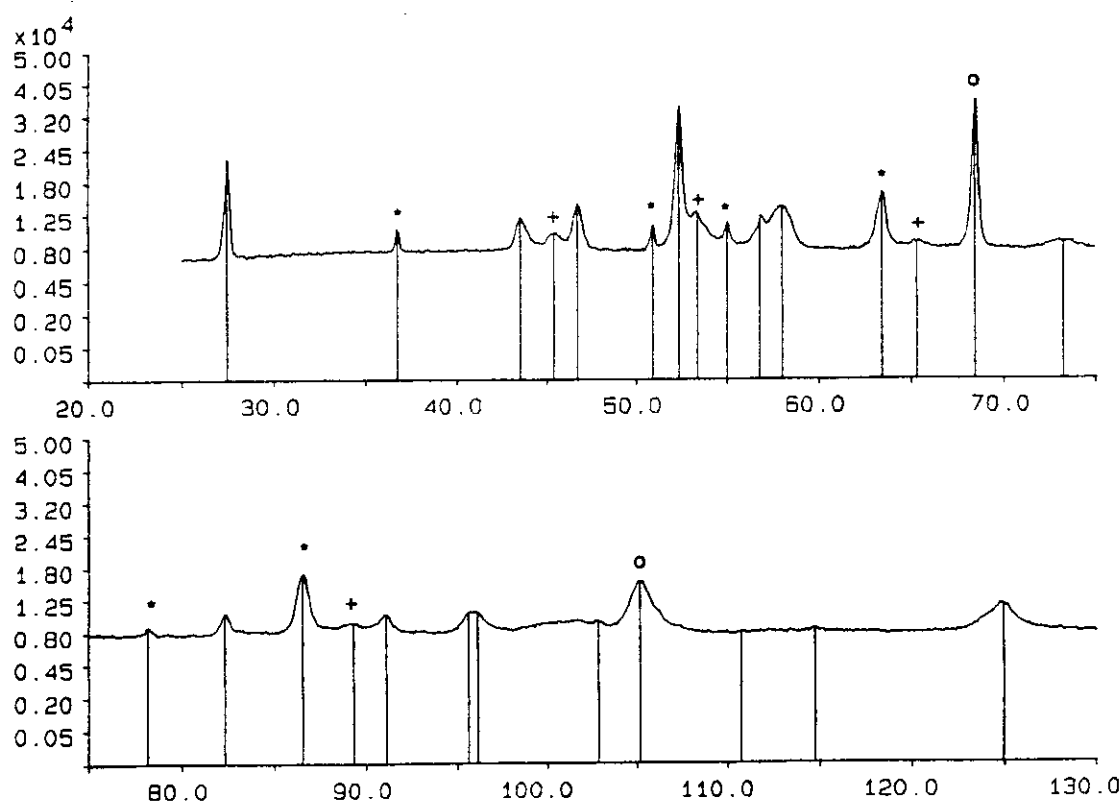

Fig. 1. Typical X-ray diffractogram of (Fe, Cr)-spinel coating on duplex SAF2205. Cubic (Fe,Cr)-spinel (sp = +) and Cr₂O₃ phases (= *), α-FeCr (= 0) are marked. The remainder peaks belong to (Fe, Cr)-spinel (dsp).
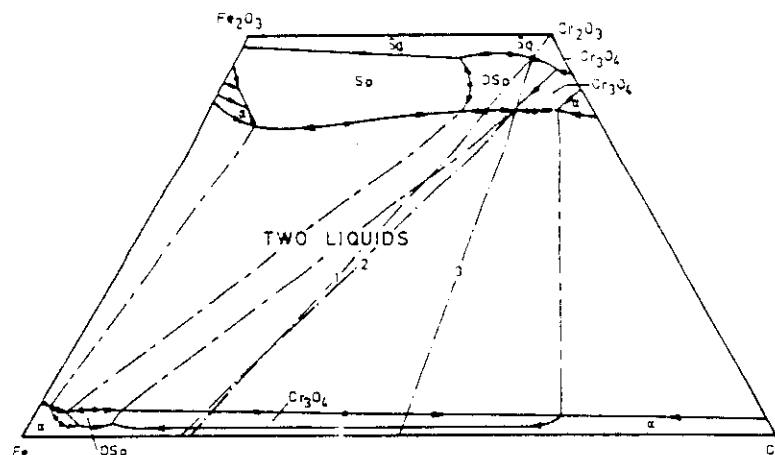
Fig. 2. Cr–Fe–O liquidus projection [3]. (1) Line of the overall starting composition. (2) Line of the phase separation in the liquid state. (3) Line of decomposition of the liquid coating material into (Fe, Cr)-spinel and α-FeCr particles.

According to the Fe–Cr–O ternary phase diagram [3], displayed in Fig. 2, the ceramic coating is formed by a phase separation in the liquid state between a oxygen rich (L_o) and a metal rich (L_m) liquid. The solidification of the L_o results in the formation of (Fe, Cr)-spinel and M(liq.). The monotectic reaction is given by: $MO(liq.) \rightarrow M_3O_4(sol.) + M(liq.)$ with M = Fe, Cr.M(liq.) results in a phase with α-FeCr particles dispersed in the coating.

EDS measurements indicated that the composition of the (Fe, Cr)-spinel was $Fe_{0.3}Cr_{2.7}O_4$. The composition was the same everywhere in the coating except for small differences such as $Fe_{0.25}Cr_{2.75}O_4$ on a 10 μm scale due to the continuous addition of Cr_2O_3-particles to the coating. According to [3] the (Fe, Cr)-spinels with composition $Fe_xCr_{(3-x)}O_4$ $(x < 1)$ are tetragonally distorted as is observed in our experiments. Under slow-cooling conditions the tetragonally distorted (Fe, Cr)-spinel decomposes into sesquioxide (M_2O_3) and metal at a temperature around 1500°C. In the present case, however, the distorted spinel phase is stabilized by cooling rates in the order of 10^5°C/s [4].

The measured lattice parameters for the (Fe,Cr)-spinel on duplex SAF2205 are listed in Table 2 together with the measured lattice parameters for the (Fe, Cr)-spinel on Fe–22 wt% Cr.

Lattice parameters could not be calculated with higher accuracy. In the case of the cubic (Fe, Cr)-spinel the accuracy was limited by the small amount of cubic spinel being present. As a result only the most predominant peaks are visible in the X-ray diffraction spectra. The accuracy of the data for the

distorted (Fe, Cr)-spinel was limited by the widths of the X-ray diffraction peaks. This peak broadening is caused by the high strain values and a high concentration of defects in the distorted spinel phase.

As can be seen from the calculated lattice parameters the lattice parameters of the (Fe, Cr)-spinel phases change if a different substrate metal was used even though the ratio of Fe to Cr is the same in both metals. This difference is attributed to the additional alloying elements which are present in the duplex SAF2205. It is known [5, 6] that the addition of Ni and Mn to the (Fe, Cr)-spinel can change the lattice parameter and even may cause a tetragonal distortion. EDS measurements indicated the presence of 4 at.% Mn in the coating on SAF2205 causing the distorted (Fe, Cr)-spinel to become more tetragonal keeping the volume constant. Ni was not detected inside the coating.

3.2. Optical microscopy

Cross sectional optical microscopy showed that a ceramic coating with a thickness of the order of 100 μm was formed on the steel substrate by the laser cladding. The coating contained no cracks parallel to the metal–ceramic interface. Instead, cracks running from the top to the bottom were observed that were concentrated in the heat affected zone near the edge of the laser track.

When SAF2205 was used as a substrate a dendritical solidification structure was observed in the coating [4]. Etching in modified Groesbeck's reagent revealed the dendrites. The dendrites are attributed to Si in the coating [4]. Etching also revealed parallel dark and bright lines in the dendrites (Fig. 3). Near the interface the lines were orientated as much as possible parallel to the interface and in the dendrites the lines were mostly at 45° to the main branch of the dendrite but other orientations were also observed.

In Fe–22 wt% Cr as a substrate no dendritical solidification structure was observed [4] and the etch

Table 2. Measured lattice parameters of (Fe, Cr)-spinel on duplex SAF2205 and on Fe–22 wt% Cr. Index sp refers to spinel and dsp to distorted spinel (units nm)

	a_{sp}	Vol_{sp}	a_{dsp}	c_{dsp}	Vol_{dsp}
SAF2205	0.835	0.583	0.616	0.777	0.295
Fe–22Cr	0.836	0.584	0.610	0.789	0.294

Table 3. The lattice parameters of the (Fe, Cr)-spinel coating on duplex SAF2205

	$(220)_{dso}$	$(400)_{so}$	$(004)_{dso}$	$(004)_{so}$
nm	0.220	0.210	0.197	0.212

Fig. 3. X-sectional optical micrograph of etched (Fe,Cr)-spinel coating on duplex SAF2205 showing dendrites orientated vertically in the coating. Holes are from etched out z-FeCr particles. Etch lines are visible. Etched in modified Groesbeck's reagent.

lines were more or less randomly orientated in the coating.

3.3. Electron microscopy

Transmission electron microscopy revealed similar microstructures in the coating on duplex SAF2205 and Fe–22 wt% Cr. The principal feature was the

plate like structure of most of the material. These plates were shown by electron diffraction to have the distorted spinel structure. In general the plates were found in two kinds of morphologies.

In one morphology the distorted (Fe, Cr)-spinel plates were found as lenticular plates embedded in a cubic (Fe, Cr)-spinel matrix (Fig. 4). The $B = [100]_{sp}$ diffraction pattern shows diffraction spots from the distorted as well as from the cubic spinel phase. The axis of the distorted spinel was rotated with respect to the axis of the cubic spinel: the angle between $(004)_{sp}$ and $(004)_{dsp}$ was $2.0°$ and between $(400)_{sp}$ and $(220)_{dsp}$ was $1.8°$. From trace analysis the macroscopic habit plane of the distorted spinel was found to be $(0.073-0.67)_{sp}$. On a microscopic scale the habit plane seemed to be segmented into planes of $(01 - 1)_{sp}$ orientation. From the diffraction pattern it is seen that the fit on $(01 - 1)_{sp}$ is very good. In Fig. 4(a) plates approximately parallel to $(01 - 1)_{sp}$ and $(011)_{sp}$ are edge on. Other plates orientations are also visible, but those plates are tilted at an angle of $45°$ with respect to the plane of projection. Strain effects are visible around the smaller distorted spinel plates. The growth of plates of one orientation is impeded by plates of other orientations but in some cases plate growth continues on the other side of the impeding plate.

From the observed diffraction patterns the lattice parameters could be measured. The errors in the absolute value of these measurements might be quite large but the relative values will still be accurate. The
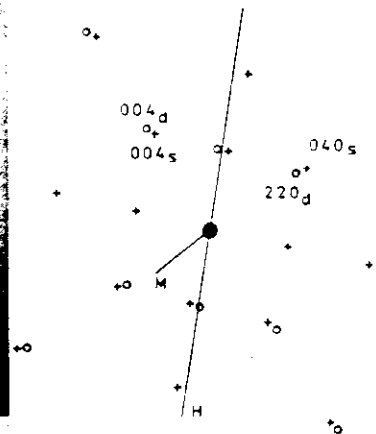

Fig. 4. Lenticular distorted spinel plates embedded in a cubic spinel matrix. Strain fields are visible around the plates. Orientation is $B = [100]_{sp}$, $B = [110]_{dsp}$. Corresponding diffraction pattern shows spots from cubic (+) as well as from distorted (o) spinel. Trace of habit plane (H) and trace of micro twins (M) are indicated. Striations are due to micro twins on $(112)_{dsp}$ planes.
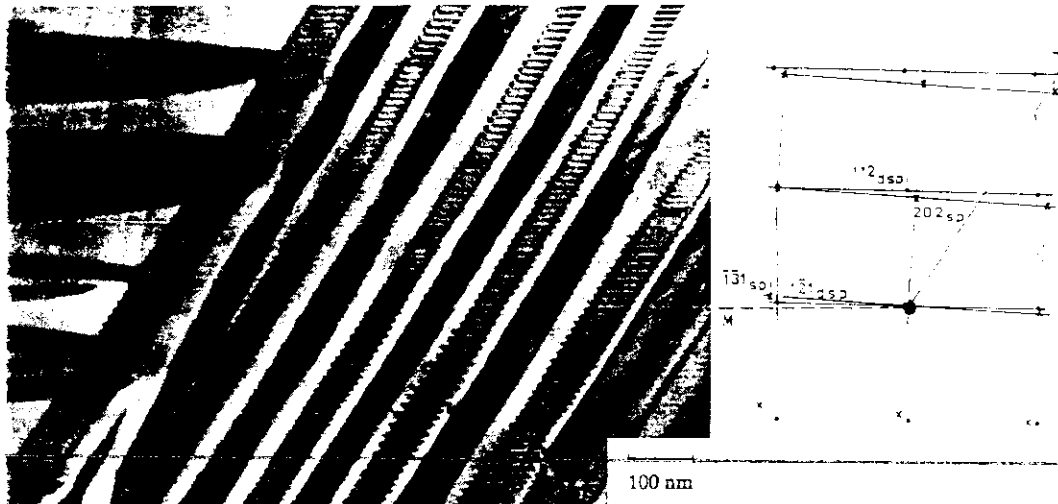
Fig. 5. Micro twins on $(112)_{dsp}$ in distorted spinel plates. If two plates intersect de-twinning occurs. The $B = [3 - 2 - 3]_{sp}$ diffraction pattern reveals spots from cubic (x) and distorted $(\bigcirc)$ spinel. Fraunhofer diffraction due to the regular (10 nm) spacing of the micro twins is visible at the $(1 - 21)_{dsp}$ spot. Traces of the microtwins (M) and of the habit plane (H) are indicated.

lattice parameters of the (Fe, Cr)-spinel coating on duplex SAF2205 are listed in Table 3.

Inside the distorted spinel plates striations were visible. Tilting to $B = [3 - 2 - 3]_{sp}$ revealed that the striations were micro twins (Fig. 5). The micro twins are on $\{112\}_{dsp}$ planes which correspond to the $\{101\}_{sp}$ planes. The twinning mechanism is a twinning with $\{112\}_{dsp}$ acting as a mirror plane: i.e. the $[001]_{dsp}$ and $[110]_{dsp}$ are interchanged over the interface. Measurements indicate that in 30–35 vol% of the distorted spinel is in the twinned orientation. The distance between the micro twins is typically 10–15 nm. It can be seen from Fig. 5 that the micro twins are not present at the location where two plates impinge. The plates seem to be de-twinned by the crossing of a

plate of different orientation. Consistent indexing of the diffraction pattern revealed that the striations in Fig. 4(a) are micro twins on $(112)_{dsp}$.

In the second plate morphology the parallel distorted (Fe, Cr)-spinel plates had completely filled the volume and no cubic spinel was found (Fig. 6). The interface plane between the adjacent distorted spinel plates is formed by a $\{112\}_{dsp}$ plane although the interface is not always perfectly flat. The adjacent plates are always in a twinned orientation and this is reflected in the traces of the micro twins (Fig. 6) which form a zigzag pattern. A regular pattern of defects is observed in the interface.

The plane of the micro twins is mirrored in the interface so looking in a $[101]_{dsp}$ directions the inter-
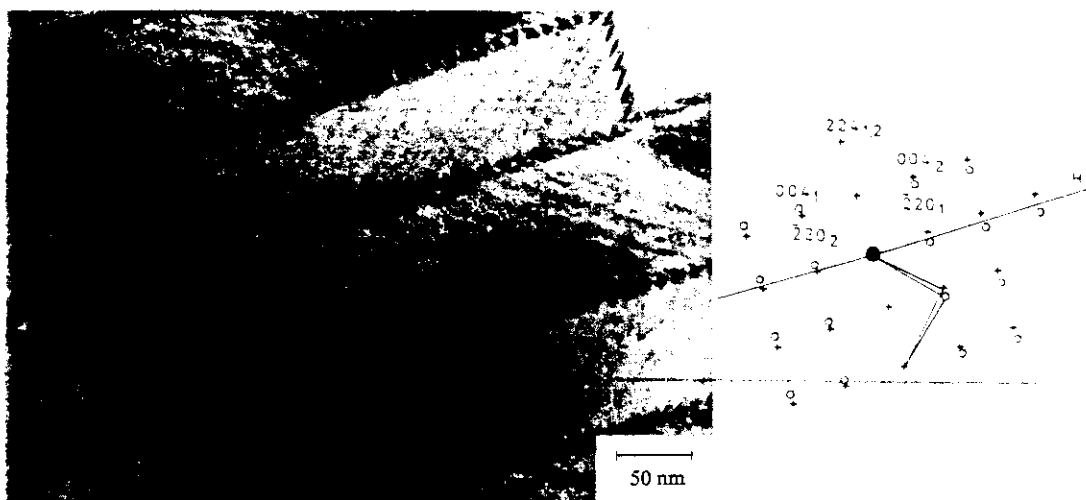

Fig. 6. Distorted spinel plates grown into contact leaving no cubic spinel in between the plates. Striations are seen to form a zigzag pattern. A regular array of defects is observed on the interface. The diffraction pattern zone axis are $B_1 = [110]_{dsp}$ and $B_2 = [-1 - 10]_{dsp}$ indicating that alternate plates have a twin orientation relationship.
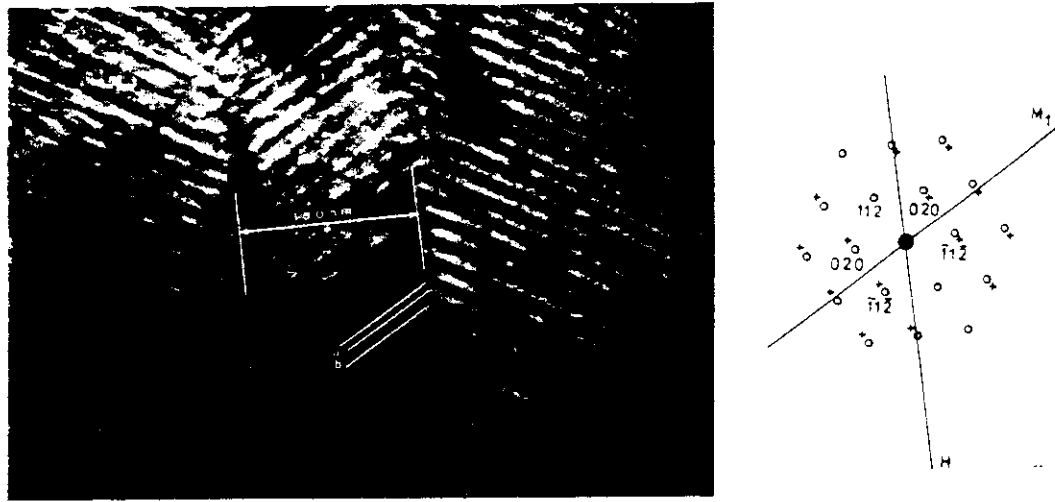
Fig. 7. Micrograph showing micro twins (a) in the plates and the interface between the plates edge on. It is observed that the micro twins are aligned where possible. The orientation of region 1 is $B_1 = [-101]_{dsp}$. The diffraction pattern shows spots due to region 1 (o) and due to the micro twinning in region 1 (+). A similar twinning relationship exists between region 1 and 2. Traces of the interface between region 1 and 2 (H) and of the micro twins in region 1 (M_1) are indicated.

face and micro twins on both sides of the interface can be edge on (Fig. 7). Where possible micro twins are aligned because the individual micro twins form a source of misfit (Fig. 8). In the micro twin the $[001]_{dsp}$ is parallel to the interface so that no twinned type of relation can exist over the interface. The only way to minimize the misfit is an ordering of the micro twins so that the micro twin is matched by another micro twin over the interface resulting in a minimal misfit. Alternate plates are mirrored in the interface plane. The micro twinning introduces a second mirroring, but on another $\{112\}_{dsp}$ plane. Because the micro twin (mirror) plane is mirrored itself the micro twinned areas are mirrored twice resulting in an
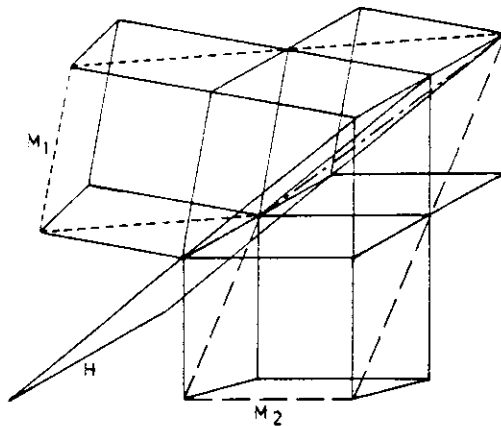

Fig. 8. Schematic drawing of twinning mechanism in distorted spinel. The solid diagonal plane is the habit plane (H) between the distorted spinel plates. The coarse dashed plane is the micro twin plane M_2 and the fine dashed plane is the micro twin plane M_1. In micro twinned area M_1 and M_2 the c-axis is coming out of the plane of the paper. The misfit is minimal when twins are aligned.

almost perfect fit over the interface when micro twins are aligned.

4. CALCULATIONS

Because most of the electron microscopic data are of the SAF2205 + Cr_2O_3 system calculations are performed for the phase transformation in this system. Similar calculations can be done for the transformation in the (Fe, Cr)-spinel, not containing Mn and the results appears to be very similar. The reason for including the (Fe, Cr)-spinel without Mn is to prove that the martensitic transformation is not caused by the addition of Mn to the spinel.

Since the lattice parameters of the cubic and the tetragonally distorted (Fe, Cr)-spinel phases are known and the twinning plane and direction are established crystallographic calculations within the framework of the phenomenological theory of martensitic transformations can be made [7, 8] based on the analysis provided by Bowles and Mackenzie (BM) [9, 10]. In order to appreciate the outcome of the calculations and keeping up with a certain coherence of the presentation some details are summarized in the following.

In any crystallographic description of an interface structure between two crystals, i.e. not typical for the phenomenological theory of martensite transformations, it is necessary to define a lattice correspondence, that correlates planes and directions of the separate structures to each other at the interface. This correspondence is described by a lattice deformation S, i.e. a homogeneous distortion of one structure to that of the other, the latter of which is factored into a pure strain B and a rigid-body rotation R:S = RB. In fact the character of S will determine the morphology and minimizes the strain energy in the

Table 4

	Solution 1	Solution 2	Solution 3	Solution 4
p_1	(0.0651, 0.7786, 0.6242)	(0.6242, 0.7786, 0.0651)	(0.0651, 0.7786, 0.6242)	(0.6242, 0.7786, 0.0651)
d_1	(0.0049, 0.0548, 0.0472)	(0.0472, 0.0548, 0.0049)	(0.0049, 0.0548, 0.0472)	(0.0472, 0.0548, 0.0049)
m_1	0.0725	0.0725	0.0725	0.0725
m_2	0.0851	0.1427	0.0851	0.1427
$/S/$	$\begin{bmatrix} 1.0423 & 0.0038 & 0.0396 \\ 0.0023 & 1.0426 & 0.0329 \\ 0.0445 & 0.0367 & 0.9291 \end{bmatrix}$	$\begin{bmatrix} 1.0400 & 0.0367 & 0.0664 \\ 0.0364 & 1.0426 & 0.0058 \\ 0.0746 & 0.0038 & 0.9282 \end{bmatrix}$	$\begin{bmatrix} 1.0423 & 0.0038 & 0.0396 \\ 0.0023 & 1.0426 & 0.0329 \\ 0.0445 & 0.0367 & 0.9291 \end{bmatrix}$	$\begin{bmatrix} 1.0400 & 0.0367 & 0.0664 \\ 0.0364 & 1.0426 & 0.0058 \\ 0.0746 & 0.0038 & 0.9282 \end{bmatrix}$
Twinning (%)	37.1208	62.2286	37.1208	62.2286
$(001)_{dsp}$	(0.0426 0.0353 0.9985)$_{co}$	(0.0713 0.0062 0.9974)$_{co}$	(0.0426 0.0353 0.9985)$_{sp}$	(0.0713 0.0062 0.9974)$_{co}$
$(110)_{dsp}$	(0.9991 0.0022 0.0427)$_{co}$	(0.9968 0.0349 0.0715)$_{co}$	(0.9991 0.0022 0.0427)$_{co}$	(0.9968 0.0349 0.0715)$_{co}$
$(1\bar{1}0)_{dsp}$	(0.0037 0.9994 0.0352)$_{co}$	(0.0352 0.9994 0.0037)$_{co}$	(0.0037 0.9994 0.0352)$_{co}$	(0.0352 0.9994 0.0037)$_{co}$

structure. As a matter of course any further reductions of the strain energy can be obtained by decreasing the net transformation strain energy, e.g. mechanical twinning and plastic deformations, that produces a change of shape without altering the lattice itself. Therefore any further deformation must lead to a lattice-invariant deformation, denoted by invariant-plane lattice deformations P_1. The macroscopic shape strain is then a product arising from the lattice deformation **RB** and lattice invariant deformations P_1. In the crystallographic theory commonly applied to martensitic transformations the net transformation strain defined by **RBP** is minimized by a plate shape that leaves a (habit) plane undistorted. As a result the macroscopic net deformation must be an invariant-plane strain.

First a lattice correspondence between the cubic and the distorted spinel phase has to be assumed, taking into account the observed orientation relationship between the two phases: $(400)_{sp}//(220)_{dsp}$ and $(004)_{sp}//(004)_{dsp}$. The correspondence matrix is taken as (f = spinel, t = distorted spinel)

$$tCf = \begin{bmatrix} \frac{1}{2} & -\frac{1}{2} & 0 \\ \frac{1}{2} & \frac{1}{2} & 0 \\ 0 & 0 & 1 \end{bmatrix}$$

In this frame of reference the $[001]_{sp}$ will be the contraction axis of the lattice (Bain) deformation. The principal distortions as calculated from the experimental data are:

$$\eta_1 = \eta_2 = \frac{\sqrt{2} \cdot a}{a_0} = 1.0433$$

$$\eta_3 = \frac{c}{a_0} = 0.9305.$$

which define the deformations **B** relative to the parent phase.

It is readily seen that for a pure lattice distortion to leave a plane invariant, the habit plane, the necessary and sufficient condition is that one of the principal distortions must be unity and of the other

two one should be larger and the second less than unity [11, 12]. Clearly **B**, as described before is inconsistent with this rule. As a consequence since **B** leaves no plane invariant, but instead leaves a line (or cones of lines) undistorted, the superposition of only a single lattice invariant shear **P** is sufficient to give a macroscopically undistorted (habit) plane. The net deformation is then described by $P_1 = RBP$, or $P_1 P_2 = RB$, where $P_2 = P^{-1}$.

P is of the form $(I - m dp')$ and represents a simple shear in the direction **d**.

m gives the magnitude of the shape deformation for a given p' and p'_1 represents the habit plane.

The product **RB** is an invariant line strain, **S**, defined by the planes that are invariant to P_2 and P_2. Once **S** is known all the crystallographic features can be calculated. The (Bain) lattice distortions are given by the lattice parameters of the various phases and the rigid body rotation **R** can be calculated once the plane p'_2 and the direction d_2 of P_2 are assumed.

The lattice invariant shear is taken as observed from the experimental data of the microtwinning. The observed type of micro twinning can only occur in the distorted spinel phase but is transferred to a shear plane p'_2 and a shear direction d_2 in the cubic spinel phase.

$$p'_2 = (101)_{sp}$$

$$d_2 = [\bar{1}01]_{sp}.$$

However in general there are two different invariant lines for a given p'_2 and d_2 specifies two planes with invariant normals. Therefore, for a given **B** and P_2 there are four different **R** and consequently four different **S**. The results of the four solutions are given in Table 4 which also lists the calculated positions of the $(110)_{dsp}$ and $(001)_{dsp}$ axis referred to the orthonormal axis of the cubic spinel. The fractional amount of twinning required to incorporate the calculated lattice invariant shear is also shown.

It can be seen from Table 4 that the solutions are degenerate. All four habit plane solutions are variants of each other. However, solutions 1 and 3 and solutions 2 and 4 involve different orientation re-

lationships. Comparison of the calculated orientation relationship with the measured angles between the axis of the cubic spinel and the distorted spinel shows that solutions 1 and 3 are in better agreement than solutions 2 and 4. Solutions 2 and 4 can thus be discarded. It should be noted that solutions 1 and 3 are also better on the basis of their lower value of m_3. A smaller value of m_3 means that less lattice invariant strain has to be accommodated. The high value of m_3 for solutions 2 and 4 is reflected in the large amount of micro twinning. For solutions 1 and 3 the calculated amounts of twinning are in excellent agreement with the experimental data. Calculated rotations between $[004]_{sp}$ and $[004]_{dsp}$ and between $[040]_{sp}$ and $[-220]_{dsp}$ are in agreement with solution 1 and 3 when the projection in the $(100)_{sp}$ plane is taken into account. The direction of rotation is in agreement with solution 1. The observed habit plane fits to the calculated solutions for p'_1.

5. DISCUSSION

In the present experiments $Fe_xCr_{(3-x)}O_4$ is found having the tetragonally distorted spinel structure. The tetragonally distorted spinels belong to the space group $I_{41/amd}$[13]. The crystal structure is similar to the spinel structure (space group F_{d3m}) with the c-axis being shorter than the a-axis. In normal spinel with the chemical composition AB_2O_4 the O^{2-} ions form an f.c.c. sublattice with A^{2+} ions in the tetrahedral and B^{3+} ions in the octahedral interstices. For indexing of diffraction patterns of the cubic spinel the f.c.c. system can be used, keeping in mind the double periodicity of the O^{2-} f.c.c. sublattice due to the fact that not all tetrahedral and octahedral sites are filled. For the indexing of the distorted spinel one should bear in mind that the [010] direction of the distorted spinel is defined parallel to the [110] of the cubic spinel. This affects the indexing of planes and directions.

The $Fe_xCr_{(3-x)}O_4$ phase is a high temperature phase that decomposes eutectoidally into Cr_2O_3 and α-(Fe, Cr) at a temperature of $1500°C$[3]. The reason for the low temperature existence of the distorted (Fe, Cr)-spinel is the cooling rates in the order of $10^5°C/s$ obtained during laser treatment[4].

The microstructure observed in TEM indicates that the material does not solidify in the distorted spinel structure. The presence of a small amount of cubic (Fe, Cr)-spinel suggests that the distorted spinel in fact might be nucleated from the cubic spinel phase. The plate like morphology of the distorted spinel phase in combination with the twinned internal structure of the plates suggests that the transformation might be martensitic. Martensitic calculations executed with the lattice parameters of the cubic and distorted (Fe, Cr)-spinel phases are in excellent agree-

ment with the experimental data confirming that the transformation might be martensitic indeed.

A similar cubic to tetragonally distorted spinel transformation is observed in Mn_3O_4 [14]. However this particular transformation is not martensitic. The reason for the difference is that in the Mn_3O_4 the a lattice parameter does not change and the c lattice parameter is elongated. This causes the (001) plane to be a lattice invariant plane.

The fully martensitic microstructure resembles the twinned microstructure that is observed in Mn_3O_4. The reason for this resemblance is the macroscopic shape retention causing the Mn_3O_4 to be internally twinned and the (Fe, Cr)-spinel to form martensitic plates in alternate orientations. When the martensitic plates grow into contact their orientation relationship is almost twinned. The shape retention is also seen in the dendritical structure of Fig. 3. The martensitic plates which are revealed as etch lines are orientated so that the invariant plane is that particular $\{101\}_{sp}$ plane which is the most difficult to rotate.

REFERENCES

1. X. B. Zhou and J. Th. M. De Hosson, *Acta metall. mater.* **39**, 2267 (1991).
2. J. Th. M. De Hosson, X. B. Zhou and M. van den Burg, *Acta metall. mater.* **40**, s139 (1992).
3. D. C. Hilty, W. D. Forgeng and R. L. Folkman, *Trans. Am. Inst. Min. Metall. Engrs.* **203**, 253 (1955).
4. M. van den Burg, J. Th. M. De Hosson, *J. Matter Sci.* (1993), Submitted.
5. G. C. Allen, J. A. Jutson and P. A. Tempest, *J. Nucl. Mater.* **160**, 34 (1988).
6. G. C. Allen, J. A. Jutson and P. A. Tempest, *J. Nucl. Mater.* **158**, 96 (1988).
7. C. M. Wayman, *Introduction to the Crystallography of Martensitic Transformations* Macmillan, New York (1964).
8. J. van Landuyt and C. M. Wayman, *Acta metall.* **16**, 803, 815 (1968).
9. J. S. Bowles and J. K. Mackenzie, *Acta metall.* **2**, 124, 129, 138 (1954).
10. G. B. Olson and M. Cohen, in *Dislocations in Solids*, (edited by F. R. N. Nabarro Vol. 17, p.295., North-Holland, Amsterdam (1986).
11. J. W. Christian, *J. Inst. Metals* **84**, 386 (1956).
12. M. S. Wechsler, D. S. Lieberman and T. S. Read, *Trans. Am. Inst. Min. Engrs* **197**, 1503 (1953).
13. C. Palache, H. Berman and C. Frondel, *Dana's System of Mineralogy*, Vol. I, p.712. Wiley, New York (1946).
14. L. A. Tietz, R. Dieckmann and C. B. Carter, *Proc. 45th Ann. Meeting of the Electron Microscopic Soc. of America*, San Fransisco Press (1987).
15. Sandvik SAF 2205, UNS S31803, Sandviken, Sweden, S-1, 874-ENG (1989).